

## Local Real-Space View of the Achiral $1T$ -TiSe<sub>2</sub> $2 \times 2 \times 2$ Charge Density Wave

B. Hildebrand,<sup>1,\*</sup> T. Jaouen,<sup>1,†</sup> M.-L. Mottas,<sup>1</sup> G. Monney,<sup>1</sup> C. Barreteau,<sup>2</sup> E. Giannini,<sup>2</sup> D. R. Bowler,<sup>3</sup> and P. Aebi<sup>1</sup>

<sup>1</sup>*Département de Physique and Fribourg Center for Nanomaterials, Université de Fribourg, CH-1700 Fribourg, Switzerland*

<sup>2</sup>*Department of Quantum Matter Physics, University of Geneva, 24 Quai Ernest-Ansermet, 1211 Geneva 4, Switzerland*

<sup>3</sup>*London Centre for Nanotechnology and Department of Physics and Astronomy, University College London, London WC1E 6BT, United Kingdom*



(Received 16 October 2017; published 30 March 2018)

The transition metal dichalcogenide  $1T$ -TiSe<sub>2</sub>-two-dimensional layered material undergoing a commensurate  $2 \times 2 \times 2$  charge density wave (CDW) transition with a weak periodic lattice distortion (PLD) below  $\approx 200$  K. Scanning tunneling microscopy (STM) combined with intentionally introduced interstitial Ti atoms allows us to go beyond the usual spatial resolution of STM and to intimately probe the three-dimensional character of the PLD. Furthermore, the inversion-symmetric achiral nature of the CDW in the  $z$  direction is revealed, contradicting the claimed existence of helical CDW stacking and associated chiral order. This study paves the way to a simultaneous real-space probing of both charge and structural reconstructions in CDW compounds.

DOI: [10.1103/PhysRevLett.120.136404](https://doi.org/10.1103/PhysRevLett.120.136404)

Transition metal dichalcogenides (TMDCs) have been extensively studied for decades, but recently, the development of methods to obtain nanosheets or even monolayers has brought renewed interest for these materials because of their attractive electronic and optoelectronic properties for applications [1,2]. Many TMDCs also undergo charge density waves (CDW) or/and superconducting phase transitions at low temperature [3–7], and recently,  $1T$ -TiSe<sub>2</sub> has been even proposed as the first TMDC exhibiting a CDW with a scalar chiral order [8,9].

Scanning tunneling microscopy (STM) probes the real-space surface electron density. Therefore, the electronic reconstruction associated with the commensurate  $2 \times 2 \times 2$  CDW of  $1T$ -TiSe<sub>2</sub> can be easily tracked in the topmost Se layer up to atomic resolution [10,11]. This local approach has indeed allowed us to propose the chirality of the CDW [8,12] and to observe the formation of phase-shifted CDW domains induced by intercalation of Ti or Cu atoms [13–16]. However, the three-dimensional (3D) character of the CDW as well as the periodic lattice distortion (PLD) accompanying the phase transition can, in principle, not be directly probed, the displacement amplitude induced by the PLD [17,18] being well below the usual spatial resolution of STM [19].

Yet, being able to obtain information about the 3D character of the CDW as well as getting insight about the PLD in real space is of fundamental interest in the context of domain formation or CDW dimensional crossover [20], but also with respect to the question of chirality, which strictly signifies a loss of inversion symmetry between two adjacent Se-Ti-Se sandwiches.

Here, the electronic signature of defects induced by the presence of interstitial Ti atoms in between Se-Ti-Se

sandwiches is exploited for probing the symmetry of the PLD. This combined STM-defect technique therefore goes beyond the resolution limitation of STM, providing access to the structural and intimate 3D nature of the  $1T$ -TiSe<sub>2</sub> CDW. Interstitial Ti defects are first recognized and characterized. A systematic asymmetry induced by the surrounding surface PLD is observed and the associated deformation is uniquely determined with the help of density functional theory (DFT) calculations. Furthermore, the potential of this new technique is highlighted through a simultaneous measurement of two adjacent Se-Ti-Se sandwiches at a step edge, where the CDW-PLD is found to display the expected commensurate  $2 \times 2 \times 2$  signature with atomic displacements, as proposed by Di Salvo *et al.* [17]. Therefore, there is no evidence of a loss of inversion symmetry, contradicting recent claims of a chiral phase [8,12].

The strength of this combined STM-defect technique also relies on its relative simplicity. Indeed, a defect density of less than 1% allows precise identification of the surface PLD. Hence, this work not only paves the way towards a better local understanding of structural reconstructions in CDW compounds, but is also highly promising for phase transition studies in general, where a local and real-space vision of entangled electronic and structural instabilities is essential.

The  $1T$ -TiSe<sub>2</sub> single crystals were grown by iodine vapor transport at 700 °C with 5% additional Ti in the growth tube with respect to perfect stoichiometric conditions. Resistivity measurements were performed by a standard four-probe method using a lock-in as current source and voltage meter. The samples were cleaved *in situ* below  $10^{-7}$  mbar at room temperature. Constant current STM images were recorded at 4.6 K using an Omicron

LT-STM, with bias voltage  $V_{\text{bias}}$  applied to the sample. Base pressure was better than  $5 \times 10^{-11}$  mbar.

DFT calculations have been performed using the plane wave pseudopotential code VASP [21,22], version 5.3.3. Projector augmented waves [23] were used with the Perdew-Burke-Ernzerhof [24] exchange correlation functional. The cell size of our model was  $28.035 \times 28.035$  Å. The 1T-TiSe<sub>2</sub> surface was modeled with two layers and the bottom Se layer fixed. A Monkhorst-Pack mesh with  $2 \times 2 \times 1k$  points was used to sample the Brillouin zone of the cell. The parameters gave an energy difference convergence of better than 0.01 eV. During structural relaxations, a tolerance of 0.03 eV/Å was applied. STM images were generated using the Tersoff-Hamann approach [25], in which the current  $I(V)$  measured in STM is proportional to the integrated LDOS of the surface using the bSKAN code [26].

Figure 1(a) shows a DFT simulation, relaxed from displacements following Di Salvo *et al.* [17], of a high-resolution low-temperature empty-state STM image of 1T-TiSe<sub>2</sub> close to  $E_F$  (small positive  $V_{\text{bias}}$ ) [11]. In addition to the  $1 \times 1$  charge density corresponding to the position of the atoms in the topmost Se layer [10], the  $2 \times 2$  CDW modulation can be identified through the succession of atoms appearing more or less intense and labeled “CDW max” [see max in Fig. 1(a)] and “CDW min” [see min in Fig. 1(a)]. The  $2 \times 2$  surface unit cell contains exactly one CDW maximum and three CDW minima [dashed rhombus in Fig. 1(a)]. In-plane displacement amplitude of the Se atoms [see  $\text{Se}_{\text{up}}$  and  $\text{Se}_{\text{down}}$  in Fig. 1(b)] corresponds to 0.028 Å at 77 K [17], which is almost 2 orders of magnitude below the highest lateral resolution reached by standard STM and can thus not be directly tracked with this technique. Interestingly, according to the PLD, the new unit cell also contains exactly one  $\text{Se}_{\text{up}}$  atom, which has not moved with respect to its normal state position, and three  $\text{Se}_{\text{up}}$ , which have undergone a small distortion. This observation demonstrates the close relationship between CDW modulation and PLD and allows us to directly associate the CDW maxima to the nondisplaced Se atoms [see  $\text{Se}_{\text{up}}$  max atoms in Fig. 1(c)] and the CDW minima to the displaced ones [see arrows on  $\text{Se}_{\text{up}}$  min atoms in Fig. 1(c)].

Nevertheless, we would like to stress that measuring the  $2 \times 2$  charge modulation with STM does not allow us to uniquely determine the *handedness* of the PLD occurring within the first Se-Ti-Se sandwich. Indeed, due to the characteristic antiphase locking of the  $2 \times 2 \times 2$  CDW between adjacent Se-Ti-Se layers [see Figs. 1(b) and 1(c)] [17], there are two possible periodic distortions [right-handed or left-handed; see Fig. 1(c)] for one CDW modulation at the surface. STM alone is therefore completely blind to this essential parameter exhibiting the 3D character of the CDW.

Figure 2(a) displays a measured large empty-state STM image close to  $E_F$  (150 mV). Many types of atomic defects can be recognized, the overall impurity density

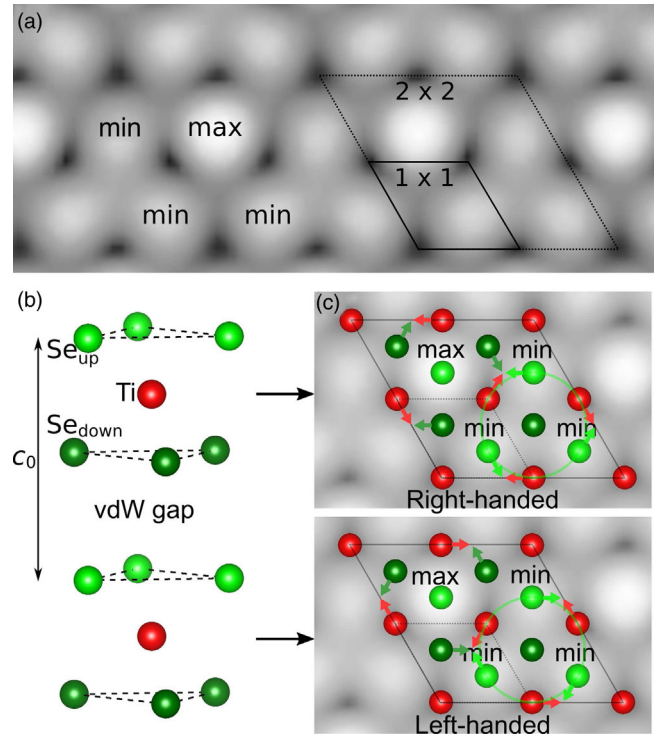


FIG. 1. (a) Simulation of the CDW as observed in STM at  $V_{\text{bias}} = 100$  mV with indication of three minima and one maximum of the charge modulation composing the  $2 \times 2$  surface unit cell. The black and the dashed rhombi indicate the  $1 \times 1$  and  $2 \times 2$  unit cells, respectively. (b) Side view of two 1T-TiSe<sub>2</sub> layers separated by a van der Waals (vdW) gap. The out-of-plane  $c_0$  lattice constant of the  $1 \times 1 \times 1$  unit cell is also shown. (c) Schematic top view of the  $2 \times 2 \times 2$  PLD corresponding to the two adjacent layers shown in (b). The arrows indicate the directions of displacement of the atoms after transition to the CDW state. The underlying modulation shows the registry of the minima and maxima of the  $\text{Se}_{\text{up}}$  layer with respect to the PLD. The two possible orientations of displacement are denominated right-handed and left-handed, respectively.

approximately corresponding to  $\approx 2\%$ . A large proportion of defects are the well-known native impurities described in a previous study [27]. Defect *A* corresponds to a Se vacancy, defects *B* and *C* are  $\text{Se}_{\text{down}}$  substitutions by iodine and oxygen atoms, respectively, and defect *D* is associated with intercalated Ti in the vdW gap. Based on surveys from STM images obtained at different regions of the sample (not shown), the density of intercalated Ti defects, which is mostly determined by the growth temperature (700 °C) [17], is  $0.57 \pm 0.07\%$  and has therefore no impact on the CDW long-range phase coherence, as seen Fig. 2(a) [13].

In addition to these four native impurities, the non-stoichiometric growth conditions have introduced another defect, never observed previously [11,27]. It stands out from the periodic and ordered Se layer as a small, bright asymmetric triangle [defect *E*, Fig. 2(a)]. The estimated density of defect *E* is  $0.79 \pm 0.08\%$ , a value close to the density of intercalated Ti [defect *D*, Fig. 2(a)]. It should not

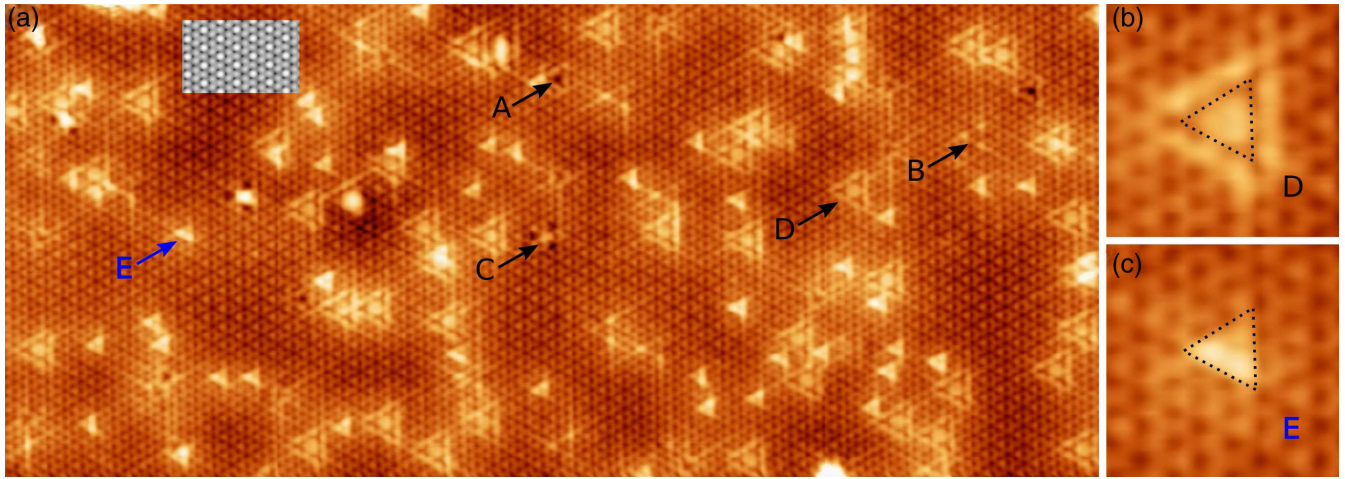


FIG. 2. (a)  $40 \times 17 \text{ nm}^2$  constant current STM image of the  $700 \text{ }^\circ\text{C}$ -grown  $1\text{T-TiSe}_2$  sample with 5% additional Ti in the growth tube.  $V_{\text{bias}} = 150 \text{ mV}$ ,  $I = 0.2 \text{ nA}$ . Native defects are labeled A–D according to Ref. [27]. The new defect is labeled E. An inset showing the DFT-simulated STM image from Fig. 1(a) is added as an eye guide; note that the image has been rotated by  $30^\circ$  with respect to Fig. 1(a). (b),(c) Enlargements on one defect of type D and E, respectively. Dotted triangles are added for highlighting the orientation of three Se atoms concerned with the electronic signatures of the defects.

be confused with the latter, which also presents a very similar small triangular shape due to enhanced density of states on top of the three neighboring  $\text{Se}_{\text{up}}$  atoms in filled states [27], below  $-0.2 \text{ V}$ . One has to keep in mind that, at this bias voltage ( $0.15 \text{ V}$ ), i.e., in empty state, the electronic perturbation induced by intercalated Ti is spatially much more extended, in such a way that the difference between defect D and E is manifest [see enlargements on both defects in Figs. 2(b) and 2(c) for comparison]. Figure 2(c) also allows us to highlight the particular asymmetric nature of the electronic signature of defect E with respect to the lattice. Indeed, two of the three topmost Se atoms concerned with its electronic perturbation are clearly brighter than the third one building a “bright edge.”

Given the special growth conditions, defect E can be reasonably attributed to additional Ti atoms. Also, the orientation of the triangular shape of defect E is identical to the central triangle of the intercalated Ti electronic signature [see small dotted triangles Fig. 2(b) and (c)]. This indicates that, as intercalated Ti, defect E is in vertical alignment with a structural Ti atom. Therefore, we performed DFT simulations of STM images in the  $2 \times 2 \times 2$  phase with an interstitial Ti atom located inside a  $\text{TiSe}_6$  octahedron forming a  $\text{Ti}_2\text{Se}_6$  structure [Fig. 3(a)]. As seen in Fig. 3(b), the DFT-simulated image for the relaxed structure at  $150 \text{ mV}$  of  $V_{\text{bias}}$  is in excellent agreement with our measurement and especially accounts for the characteristic bright edge. The arrows give the direction of displacements of the top Se atoms according to the PLD introduced in the simulation.

In particular, one of the atoms building the bright edge is a CDW maximum (nondisplaced atom) and the second bright atom corresponds to an atom that moves away from the first one according to the PLD. Comparing the

simulation to the three observed conformations of the bright edge induced by interstitial Ti atoms in Fig. 2 [see enlargements in Figs. 3(c)–3(e)] first confirms that it is always constituted of one CDW maximum [28]. Then, plotting the corresponding directions of distortion on the observed conformations [arrows in Figs. 3(c)–3(e)] uniquely demonstrates that, here, the underlying PLD is the left-handed one [Fig. 1(c)].

One has to realize that one single interstitial Ti atom defect on a STM image is already sufficient for probing the

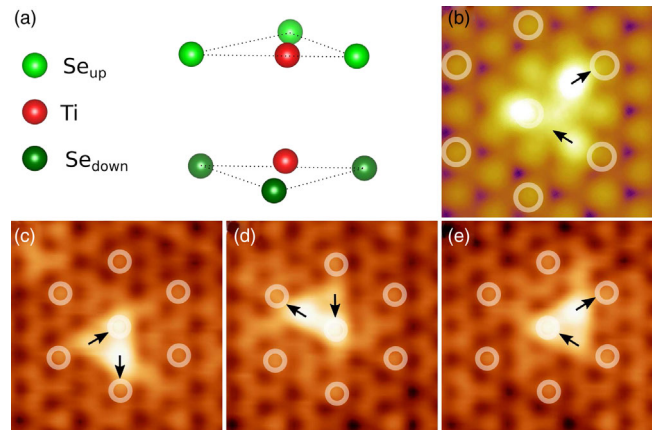


FIG. 3. (a) Side view of the DFT-calculated relaxed structure with an interstitial Ti atom. (b) DFT-simulated STM image at  $V_{\text{bias}} = 150 \text{ mV}$ . White circles mark the CDW maxima and arrows show the direction of simulated PLD displacements according to Di Salvo *et al.* [17] of the  $\text{Se}_{\text{up}}$  atoms concerned with the electronic perturbation of the defect. (c)–(e) Enlargements on three defects of type E from Fig. 2 with three different orientations. White circles again mark the CDW maxima extended from the defect-free region and arrows show the direction of PLD displacements deduced from (b).

orientation of the underlying PLD, ensuring, in turn, that the 3D character of the CDW can be probed through this novel method with minimal defect-induced disturbance. Figure 4(a) shows a STM image at a step edge between two adjacent layers separated by  $\approx 6$  Å, corresponding to one  $c_0$  lattice constant [see inset of Fig. 4(a)]. The CDW charge modulation is recognizable on both terraces and can be easily tracked. Also, two interstitial Ti defects are clearly observable on each side of the step edge [see white rectangles in Fig. 4(a)], therefore providing atomic probes of the PLD orientation for the top and bottom  $\text{TiSe}_2$  layers. Comparing the positions of the CDW maxima with the electronic signatures of the interstitial Ti atoms for both layers [see white circles on enlargements in Figs. 4(b) and 4(c)] allows for determining the direction of motion that the Se atoms have undergone through the

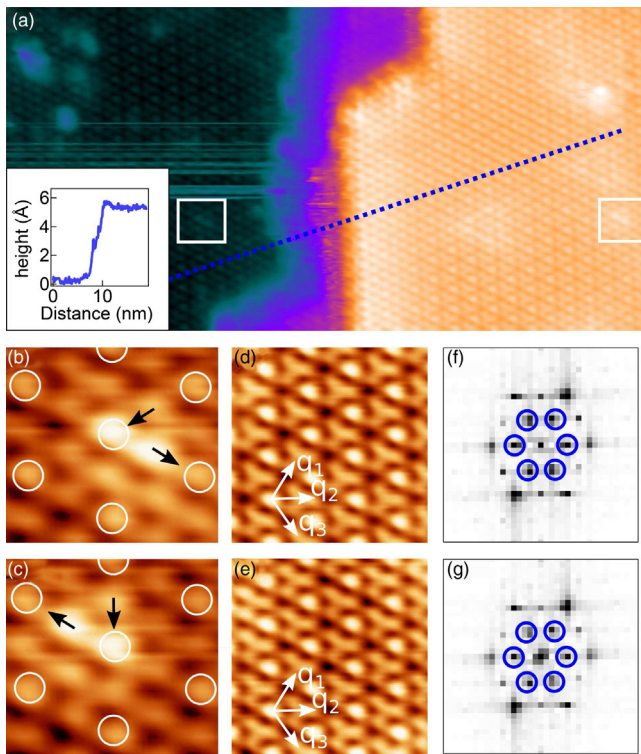


FIG. 4. (a)  $20 \times 10$  nm<sup>2</sup> constant current STM image at  $V_{\text{bias}} = 150$  mV and  $I = 0.1$  nA of two adjacent  $1T\text{-TiSe}_2$  layers. (Inset) Height difference of approximately 6 Å corresponding to the separation between two Se-Ti-Se sandwiches obtained along the profile represented by the blue dotted line. Two white rectangles indicate the presence of two defects induced by interstitial Ti, one on each layer. (b),(c) Enlargements on the defects of the bottom and top layer, respectively, with white circles indicating the position of the maxima of the CDW charge modulation and black arrows indicating the corresponding PLD-induced atomic displacements. (d),(e)  $2.8 \times 2.8$  nm<sup>2</sup> enlargements showing the CDW modulation in the bottom and top layer, respectively, with arrows indicating the orientations of the CDW  $q$  vectors. (f),(g) FFT-amplitude plots obtained from (d) and (e) with blue circles highlighting the extra spots originating from the CDW charge modulation.

phase transition [see black arrows in Figs. 4(b) and 4(c)]. The PLD is therefore found to be left handed for the top layer and right handed for the bottom [Fig. 1(c)], demonstrating that we are facing a local real-space view of the  $2 \times 2 \times 2$  character of the  $1T\text{-TiSe}_2$  CDW.

Furthermore, our experiment allows us to readily conclude on the inversion-symmetric achiral nature of the CDW as initially proposed by Di Salvo *et al.* [17]. Indeed, the recently claimed chirality of the  $1T\text{-TiSe}_2$  CDW is based on a helical stacking of the three CDW  $q$  vectors along the  $z$  direction with a  $2c/3$  interval, leading to the existence of so-called virtual layers with shifted CDW density peaks [8]. This implies different amplitudes of CDW charge modulations along the three  $q$  vectors, not only in a single layer but also between two  $c$ -separated  $\text{TiSe}_2$  layers. Two identically sized defect-free regions of both layers are selected in Fig. 4(a) and shown in Figs. 4(d) and 4(e). Their close similarity in real space already suggests that no relative phase shifts exist between the three CDW  $q$  vectors. In addition, the integrated intensities of the CDW extra spots on fast-Fourier transformed images obtained from Figs. 4(d) and 4(e) [Figs. 4(f) and 4(g)] show a negligible variation of less than 5%. This definitely confirms the conventional layer stacking in  $1T\text{-TiSe}_2$  and rules out the proposed  $2c/3$  helical CDW stacking of chiral CDW phases [8].

In summary, the combination of STM with a low density of specific buried defects has been used to uncover the periodic lattice distortion at the  $1T\text{-TiSe}_2$  surface. The potential of this new PLD-sensitive probe has been then exemplified through the measurement of the inversion of its handedness at a step edge, therefore providing a real-space view of the  $2 \times 2 \times 2$  character of the CDW. The inversion-symmetric nature of the CDW in the  $z$  direction has been finally confirmed, contradicting the existence of CDW helical stacking and associated chiral order. In principle, this new method could be easily extended to the analysis of the mixed CDW-superconducting state in Cu intercalated  $1T\text{-TiSe}_2$  [14], as well as to other materials exhibiting phase transitions for which a better understanding of the interplay between electronic and structural degrees of freedom is required.

This project was supported by the Fonds National Suisse pour la Recherche Scientifique through Div. II. We would like to thank C. Monney, C. Renner, and M. Spera for motivating discussions. Skillful technical assistance was provided by F. Bourqui, B. Hediger, and O. Raetz.

B. H. and T. J. equally contributed to this work.

\*Corresponding author.  
baptiste.hildebrand@unifr.ch

†Corresponding author.  
thomas.jaouen@unifr.ch

[1] M. Chhowalla, H. S. Shin, G. Eda, L.-J. Li, K. P. Loh, and H. Zhang, *Nat. Chem.* **5**, 263 (2013).

- [2] Q. H. Wang, K. Kalantar-Zadeh, A. Kis, J. N. Coleman, and M. S. Strano, *Nat. Nanotechnol.* **7**, 699 (2012).
- [3] R. L. Withers and J. A. Wilson, *J. Phys. C* **19**, 4809 (1986).
- [4] A. H. Castro Neto, *Phys. Rev. Lett.* **86**, 4382 (2001).
- [5] L. Fang, P. Zou, Y. Wang, L. Tang, Z. Xu, H. Chen, C. Dong, L. Shan, and H. Wen, *Sci. Technol. Adv. Mater.* **6**, 736 (2005).
- [6] U. Chatterjee, J. Zhao, M. Iavarone, R. Di Capua, J. P. Castellán, G. Karapetrov, C. D. Malliakas, M. G. Kanatzidis, H. Claus, J. P. C. Ruff, F. Weber, J. van Wezel, J. C. Campuzano, R. Osborn, M. Randeria, N. Trivedi, M. R. Norman, and S. Rosenkranz, *Nat. Commun.* **6**, 6313 (2015).
- [7] Y. I. Joe, X. M. Chen, P. Ghaemi, K. D. Finkelstein, G. A. de la Peña, Y. Gan, J. C. T. Lee, S. Yuan, J. Geck, G. J. MacDougall, T. C. Chiang, S. L. Cooper, E. Fradkin, and P. Abbamonte, *Nat. Phys.* **10**, 421 (2014).
- [8] J. Ishioka, Y. H. Liu, K. Shimatake, T. Kurosawa, K. Ichimura, Y. Toda, M. Oda, and S. Tanda, *Phys. Rev. Lett.* **105**, 176401 (2010).
- [9] J.-P. Castellán, S. Rosenkranz, R. Osborn, Q. Li, K. E. Gray, X. Luo, U. Welp, G. Karapetrov, J. P. C. Ruff, and J. van Wezel, *Phys. Rev. Lett.* **110**, 196404 (2013).
- [10] C. G. Slough, B. Giambattista, A. Johnson, W. W. McNairy, C. Wang, and R. V. Coleman, *Phys. Rev. B* **37**, 6571 (1988).
- [11] A. M. Novello, B. Hildebrand, A. Scarfato, C. Didiot, G. Monney, A. Ubaldini, H. Berger, D. R. Bowler, P. Aebi, and C. Renner, *Phys. Rev. B* **92**, 081101(R) (2015).
- [12] M. Iavarone, R. Di Capua, X. Zhang, M. Golalikhani, S. A. Moore, and G. Karapetrov, *Phys. Rev. B* **85**, 155103 (2012).
- [13] B. Hildebrand, T. Jaouen, C. Didiot, E. Razzoli, G. Monney, M.-L. Mottas, A. Ubaldini, H. Berger, C. Barreateau, H. Beck, D. R. Bowler, and P. Aebi, *Phys. Rev. B* **93**, 125140 (2016).
- [14] S. Yan, D. Iaia, E. Morosan, E. Fradkin, P. Abbamonte, and V. Madhavan, *Phys. Rev. Lett.* **118**, 106405 (2017).
- [15] B. Hildebrand, T. Jaouen, C. Didiot, E. Razzoli, G. Monney, M.-L. Mottas, F. Vanini, C. Barreateau, A. Ubaldini, E. Giannini, H. Berger, D. R. Bowler, and P. Aebi, *Phys. Rev. B* **95**, 081104 (2017).
- [16] A. M. Novello, M. Spera, A. Scarfato, A. Ubaldini, E. Giannini, D. R. Bowler, and C. Renner, *Phys. Rev. Lett.* **118**, 017002 (2017).
- [17] F. Di Salvo, D. Moncton, and J. Waszczak, *Phys. Rev. B* **14**, 4321 (1976).
- [18] X.-Y. Fang, H. Hong, P. Chen, and T.-C. Chiang, *Phys. Rev. B* **95**, 201409 (2017).
- [19] C. J. Chen, *Introduction to Scanning Tunneling Microscopy* (Oxford University Press, New York, 2008), 2nd ed., p. 423.
- [20] P. Chen, Y.-H. Chan, X.-Y. Fang, S.-K. Mo, Z. Hussain, A.-V. Fedorov, M. Y. Chou, and T.-C. Chiang, *Sci. Rep.* **6**, 37910 (2016).
- [21] G. Kresse and J. Hafner, *Phys. Rev. B* **47**, 558 (1993).
- [22] G. Kresse and J. Furthmüller, *Phys. Rev. B* **54**, 11169 (1996).
- [23] G. Kresse and D. Joubert, *Phys. Rev. B* **59**, 1758 (1999).
- [24] J. P. Perdew, K. Burke, and M. Ernzerhof, *Phys. Rev. Lett.* **77**, 3865 (1996).
- [25] J. Tersoff and D. R. Hamann, *Phys. Rev. Lett.* **50**, 1998 (1983).
- [26] W. Hofer, *Prog. Surf. Sci.* **71**, 147 (2003).
- [27] B. Hildebrand, C. Didiot, A. M. Novello, G. Monney, A. Scarfato, A. Ubaldini, H. Berger, D. R. Bowler, C. Renner, and P. Aebi, *Phys. Rev. Lett.* **112**, 197001 (2014).
- [28] Interstitial Ti atoms can also be situated in such a way that the three atoms composing its triangular shape are three minima of the CDW modulation. Even though a detailed analysis of this conformation has been done, it is not presented here since the measurement as well as the calculation show that, for this specific case, the asymmetry is only weak and not well defined, due to the perfectly symmetric nature of its position with respect to the CDW-PLD. Hence, in this position, with respect to the lattice, interstitial Ti cannot be used as a probe of the PLD. For more precisions about the PLD-induced inequivalent conformations of single-atom defects, see Refs. [11,15].